https://doi.org/10.1016/j.diamond.2017.01.019

Diamond wheel wear mechanism and its impact on the surface generation in parallel diamond grinding of RB-SiC/Si

Quanli Zhang [1,2], Qingliang Zhao[1]*, Suet To[2], Bing Guo[1] and Wenjie Zhai[1]

[1] Centre for Precision Engineering, School of Mechatronics Engineering, Harbin Institute of Technology, Harbin, 150001, China

[2] State Key Laboratory of Ultra-precision Machining Technology, The Hong Kong Polytechnic University, Hong Kong, China

*corresponding author (email: zhaoqingliang@hit.edu.cn)

ABSTRACT

The diamond wheel wear mechanism and its impact on the surface generation of RB-SiC/Si carbide under parallel grinding was investigated. The machined surface was mainly characterized by surface fracture and diamond grits scratched plastic grooves, and the surface finish of the machined RB-SiC/Si improved with decreasing feed rate. But the non-uniform surface appeared due to the varied material removal rate at different radial position for a certain workpiece. Both macro- and micro-wheel wear occurred during grinding, and the macro-wheel wear appeared in the form of profile deviation and rapid loss of sharp edge, which contributed to the appearance of cone shape at the center of workpiece. Power spectrum analysis by Fast Fourier Transformation (FFT) confirmed the significant influence of micro wheel wear on surface generation, which involved random diamond grit splintering, abrasive flattening, grain dislodgement and graphitization.

Keywords: Wheel wear; Diamond grinding; RB-SiC/Si; Surface generation

1 Introduction

Hard and brittle materials that could serve at harsh environment, such as high temperature, high pressure and corrosive environment, are extensively utilized in optical moulding fields [1], nuclear installation [2], aeronautics and astronautics [3, 4]. Reaction-bonded SiC/Si (RB-SiC/Si) carbide is one of the typical materials [5], in which the remnant Si is added in the green body and the chemical reaction between the liquid Si with carbon during sintering process could densify the bulk material and improve the mechanical properties. Ultra-precision grinding is regarded as one of the most appropriate methods to machine these brittle materials [1, 6]. However, the diamond wheel wear is inevitable during the machining process, which has great impact on the nanometric surface characteristics [7-9]. The wheel wear is divided into micro wear and macro wear, which refers to the wear on the grain level and the deterioration of the macro geometry, respectively [7]. It was reported that the wear of grinding wheel, including the dull of diamond grits and the size deviation of wheel [8, 10], would not only affect the surface roughness but also the form accuracy of the workpiece [9, 11, 12]. Specifically, the flattening of diamond grits could increase the frictional effects and thermal loading due to decreasing number of the cutting edges involved in the material removal [13], while the macro wheel wear also had great influence on the surface form accuracy and surface roughness [11, 14], especially for the grinding in parallel mode. Although the wheel wear mechanism has been widely investigated [7, 8, 15, 16], a limited number of studies which focused on the impact of diamond wheel wear on the nanometric surface generation during parallel diamond grinding of RB-SiC/Si have been reported [11, 14].

To further address this problem, parallel diamond grinding of RB-SiC/Si carbide with a high spindle speed was performed to investigate the impact of wheel wear on

the surface formation mechanism in the present work. The nanometric surface characteristics, including the nanometric surface finish and the nanometric waviness, of RB-SiC/Si under different grinding parameters were firstly analyzed and discussed. Then, the diamond wheel wear mechanism and its impact on the nanometric surface characteristics are explored.

2 Materials and methods

2.1 Machining and materials

Parallel diamond grinding with high spindle speed was performed on Nanotech 450UPL (Moore Nanotech, USA) with minimum quantity lubrication (MQL). Commercially available Clairsol 350 (Haltermann Carless USA Inc.) is used as coolant, which is composed of petroleum distillates (hydrotreated light, kerosene-unspecified 60-100%). The grinding process is illustrated in Fig. 1, and the detail grinding parameters are listed in Table 1.

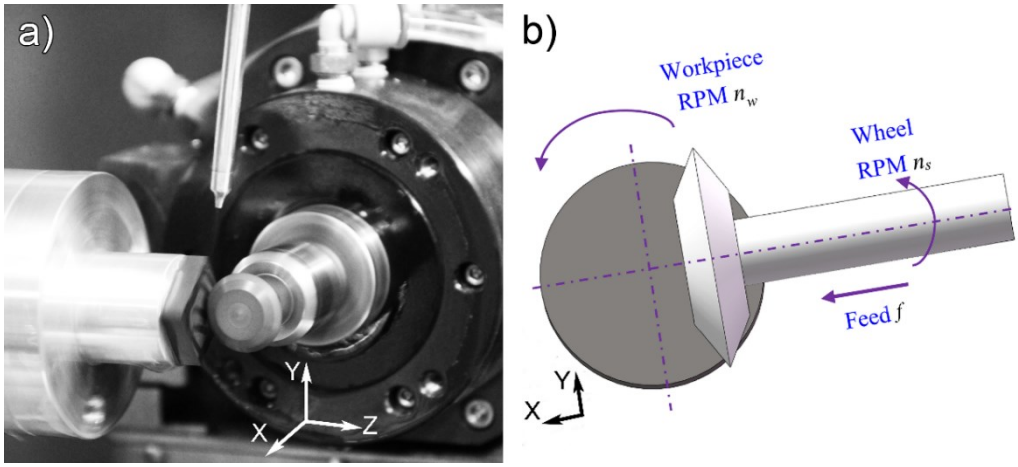

Fig. 1 Illustration of the (a) grinding setup; (b) parallel grinding mode

Table 1 Detail grinding parameters

325# W/60° diamond wheel	diam. 20 mm, resin bonded
Wheel rotational speed n_s (rpm)	20,000
Workpiece rotational speed n_w (rpm)	120
Feed rate f (mm/min)	5, 3, 1, 0.5, 0.1
Depth of grinding a_e (μm/pass)	2
Coolant	CLAIRSOL 350 (MQL)
Workpiece size (mm)	16×16×5

A thin diamond wheel with a 60° sharp edge was utilized to machine RB-SiC/Si. At a high grinding spindle speed and finer grinding parameters, the contact area between the diamond wheel and the machined workpiece surface could be seen as constant point. Therefore, it is named as “Quick point grinding”. In addition, commercially available RB-SiC/Si carbide (Goodfellow Cambridge Ltd., UK) was used as workpiece material, and the typical material properties could be found in our previous study [17].

2.2 Measurement and characterization

The cross sectional profile and arithmetic mean roughness (R_a) of the ground RB-SiC/Si surface were measured by a contact profilometer (Talysurf PGI 1240) across the workpiece center roughly. The 3D topography of the machined surface was characterized by a non-contact white light interferometer (Zygo Nexview), and the surface morphology of the machined RB-SiC/Si was characterized by a scanning electron microscope (JEOL Model JSM-6490). The edge profile of the diamond wheel after grinding was firstly observed by an optical microscope (Olympus BX60) to illustrate the macro wheel wear. In addition, the surface topography of the worn wheel edge was also examined by the white light interferometer (Zygo Nexview) and a scanning electron microscope (Hitachi TM3000) after the grinding experiment at the feed rate of 3 mm/min for 20 grinding passes.

3 Results and discussion

3.1 Surface Characteristics of the machined surface

The cross sectional profile of RB-SiC/Si after grinding is shown in Fig. 2. It can be easily seen that the average amplitude ($\triangle H$) machined at the feed rate of 5 mm/min, 3 mm/min, 1 mm/min, 0.5 mm/min, 0.1 mm/min is around 1.2 μm, 0.6 μm, 0.4 μm, 0.25 μm and 0.2 μm, respectively. Gradual improvement is achieved with decreasing

feed rate. Moreover, it can also be found that the surface profile height varied at different radial position for a certain workpiece, as shown in Fig. 2. Specifically, the surface fluctuation amplitude rises with increasing radial distance for the machined surface, which is in consistence with the increasing surface roughness (R_a) at a bigger radial distance [17]. The varied material removal rate Q_w should account for the non-uniform surface finish at different radial position, which is given by Eq. (1):

$$Q_w = a_e \cdot v_w \cdot f_r = a_e \cdot \frac{\pi \cdot r \cdot n_w}{1000 \times 60} \cdot f_r \tag{1}$$

where a_e is the depth of grinding, v_w is the linear speed of workpiece, f_r is the feed per revolution, r is the radial distance from center, and n_w is the rotational speed of the workpiece. Generally, the higher material removal rate, the rougher surface obtained [18]. Correspondingly, the average surface roughness R_a also dropped with the decrease of feed rate, as shown in Fig. 3, but the effect became insignificant as it reached 0.5 mm/min.

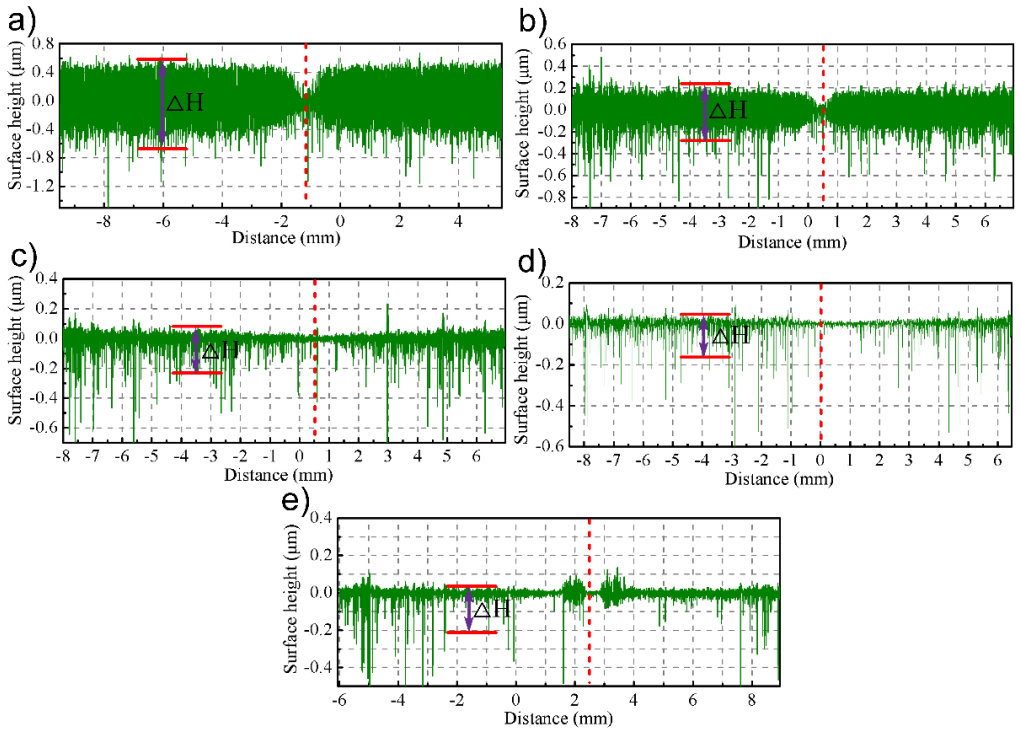

Fig. 2 Surface profile of the machined RB-SiC/Si at varied feed rate: (a) 5 mm/min; (b) 3 mm/min; (c) 1 mm/min; (d) 0.5 mm/min; (e) 0.1 mm/min

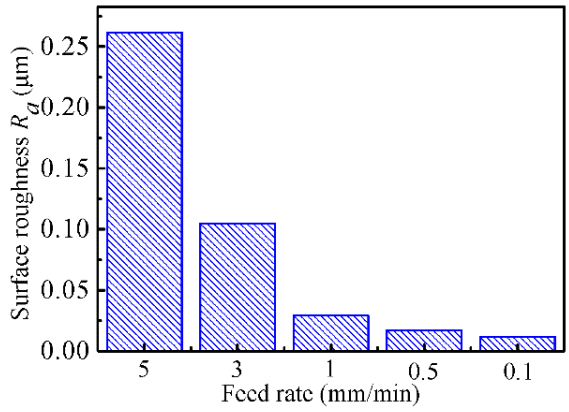

Fig. 3 The average surface roughness (R_a) of RB-SiC/Si after grinding obtained by Talysurf 1240

To get a further insight into the surface characteristics, the typical surface morphology of the workpiece after grinding at 3 mm/min and 0.1 mm/min was shown in Fig. 4. It can be readily seen that the surface was mainly covered by pulverization of SiC grains and the phase boundaries at the feed rate of 3 mm/min, which was attributed to their high brittleness [19]. Besides, the scratched plastic grooves in the grinding direction could be found on the machined surfaces. Nevertheless, only obvious micro-pits of varied size were induced and distributed randomly along the phase boundaries of SiC and Si at the feed rate of 0.1 mm/min, as shown in Fig. 4(b). This corresponded well with the stochastic protrusion height of diamond grits in wheel. Previous investigations reported that plastic deformation (mild wear) would be initiated firstly under the dynamic pressure during grinding, and then it would transform to the micro-fracture (severe wear), with the increasing contact pressure and sliding speed [20, 21]. In the present work, the typical grinding surface characteristics did transform from scratched grooves to surface fracture as the feed rate gradually increased. The serious surface fracture at a higher feed rate was attributed to the greater grinding force as it was in proportion to the material removal rate.

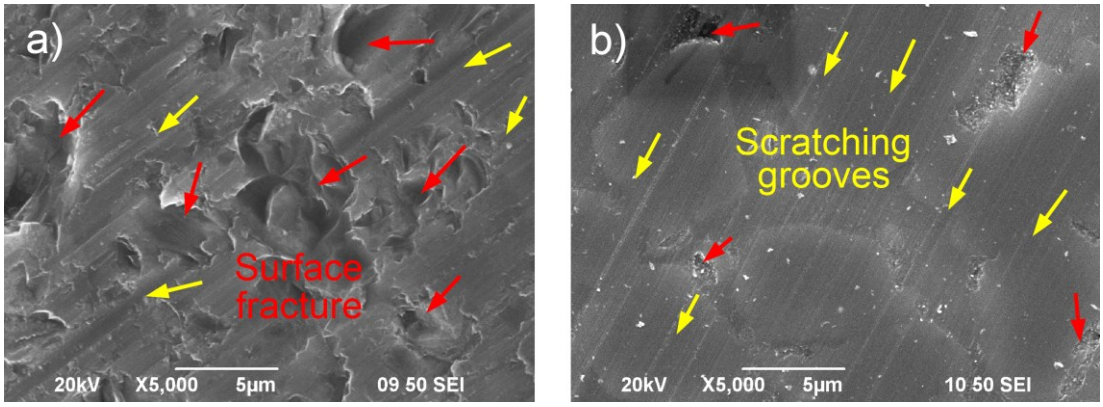

Fig. 4 SEM images of the machined surface of RB-SiC/Si at the feed rate of: (a) 3 mm/min, (b) 0.1 mm/min

3.2 Micro wheel wear mechanism and its impact

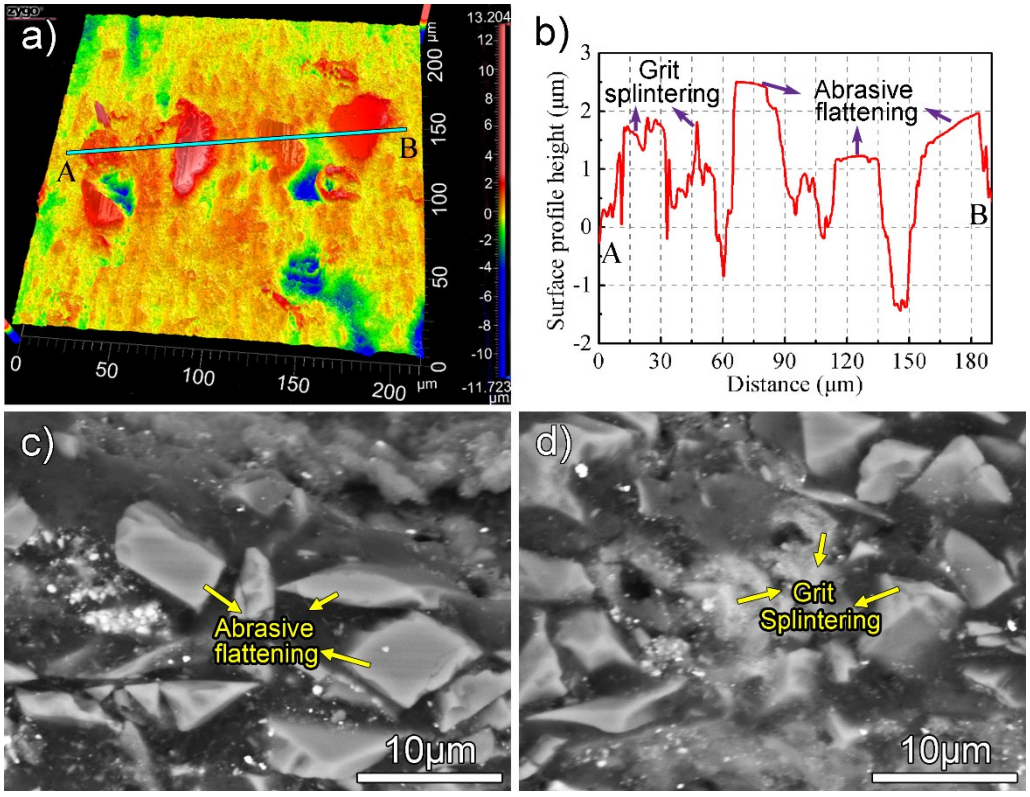

Fig. 5 (a) Surface topography of the worn wheel, (b) cross sectional profile of the worn wheel, (c) and (d) surface morphology of the diamond wheel after grinding at 3 mm/min

As shown in Fig. 5, the micro wheel wear involved diamond grits splintering, flattening and dislodgement. The random splintering and grooving worn edges of the diamond grits participated in the material removal during the grinding process, which could lead to the formation of grooves in various depth. It has been reported that the

micro fracture of the grits in the wheel resulted in the increasing number of cutting edges [8]. Axinte et al [22] studied the influence of the grit shape on the material removal mechanism, and the results revealed that the increasing number of cutting edges contributed to the ductile material removal in grinding brittle materials. On the contrary, the flattening of the diamond grits increases the frictional effects and thermal loading due to the decreasing number of cutting edges involved in material removal [13]. Therefore, graphitization of the diamond grits could be caused by the high pressure and temperature during the interaction process of diamond grits and workpiece [16, 23], which is also identified by Raman spectroscopy, as shown in Fig. 6.

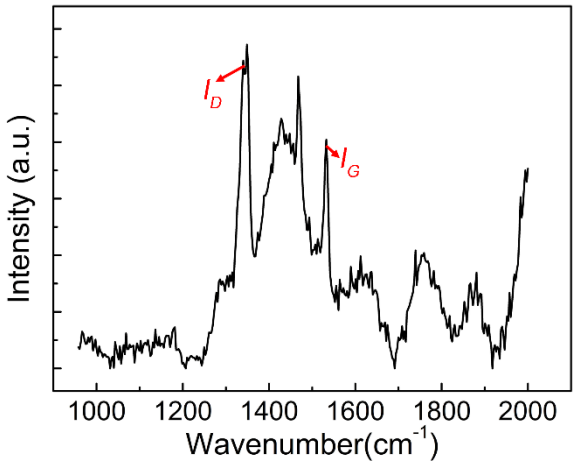

Fig. 6 Raman spectrum of the diamond wheel after grinding

To analyze the effect of micro-wear on the nanometric surface characteristics, a Fast Fourier Transformation (FFT) based Matlab program was purposely developed to process the obtained cross-sectional data by Talysurf 1240, and the results of power spectrum analysis are shown in Fig. 7. As known, the tool feed could cause period marks on the machined surface, and it contributes to a specific spatial frequency after the FFT treatment, while the theoretical spatial frequency of the tool feed component can be obtained by Eq. (2),

$$V_f = \frac{1}{f_r} \tag{2}$$

where V_f is the theoretical spatial frequency of the tool feed (1/mm), f_r is the feed per revolution (mm).

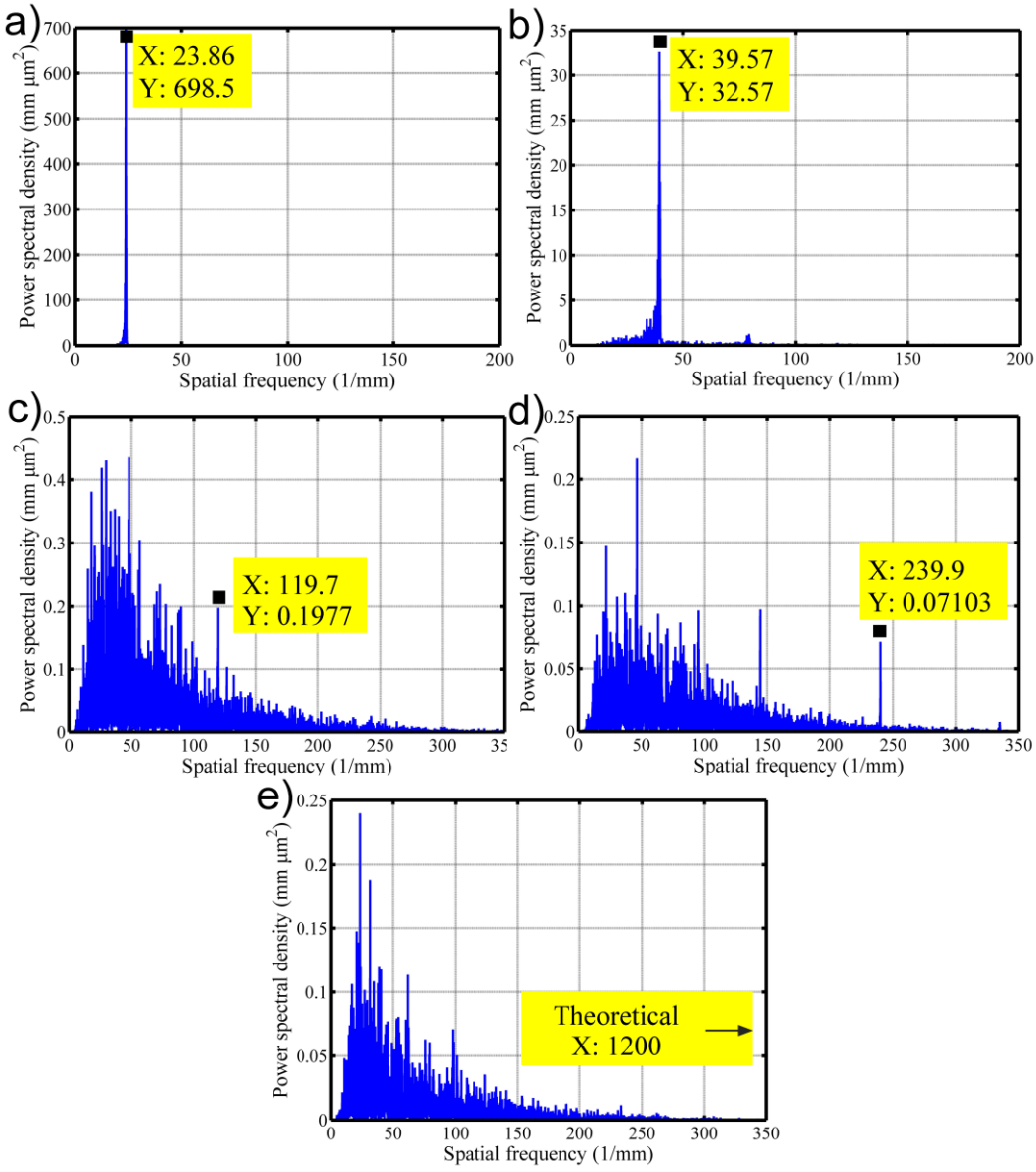

Fig. 7 Power spectrum analysis of the surface profile shown in Fig. 2 by FFT: (a) 5 mm/min; (b) 3 mm/min; (c) 1 mm/min; (d) 0.5 mm/min; (e) 0.1 mm/min

It can be readily seen that the spatial frequency of the tool feed is quite obvious for the surface machined at a higher feed rate (f>3 mm/min). However, with the decrease of feed rate, cluster spatial frequency forms around the spatial frequency of

the tool feed, which depends on the relative size of the diamond grits (d_g) with the feed per revolution (f_r). The mean diameter of the diamond grits for the 325# diamond wheel can be estimated to be around 31.7 μm by Eq. (3) [24]:

$$d_g = 28.9 \cdot g^{-1.18} \tag{3}$$

where d_g is the mean grain diameter (μm) and g is the grain size number (#).

The micro wheel wear, including the micro fracture and grooving of the diamond grits, resulted in the formation of many cutting edges on the diamond grits, but the stochastic distribution of the diamond grits and the random fracture led to the non-uniformly distributed cutting edges, the width of which is smaller than the grain diameter. However, the random distribution and generation of the cutting edges make it impossible to quantitatively describe their size during the grinding process. Therefore, we can only compare the average size of the diamond grits and the feed per revolution to explain the impact of the micro wheel wear. When f_r is greater or roughly equal to d_g, as shown in Fig. 8(a), the spatial frequency of tool feed is determined by the feed per revolution (f_r), where a residual height of material remained between the two neighboring cycle of the tool feed and the peak to valley value (PV) induced by the tool feed could be obviously found. However, when f_r becomes obviously smaller than d_g, as shown in Fig. 8(b), the surface topography of the diamond grits plays a deterministic role on the surface characteristics [10]. In addition, the random surface fracture and formation of micro-pits also contributed to the appearance of some low spatial frequency [17, 25]. Therefore, cluster spatial frequency (at around ~ 25 1/mm) of the machined surface appears, leading to the decline of the typical spatial frequency of tool feed.

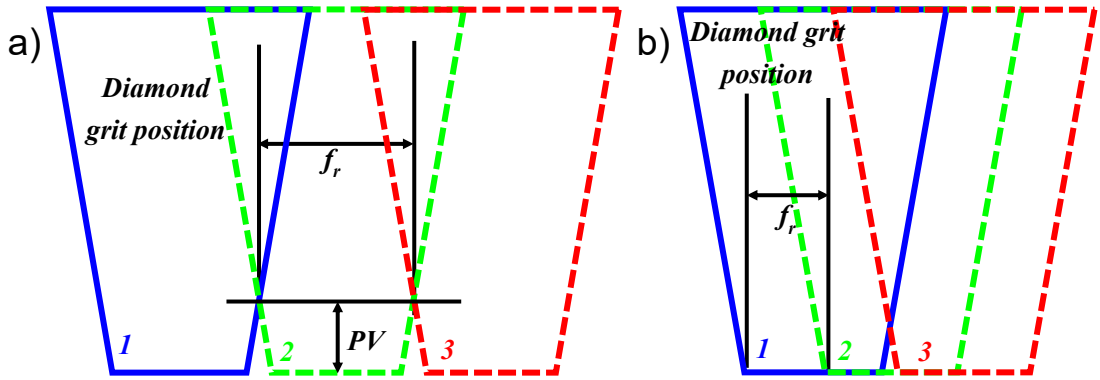

Fig. 8 The influence of the relative size of the feed per revolution and the diamond grit

3.3 Macro wheel wear and its effects on surface generation

Fig. 9(a) and (c) show the 3D center surface topography, while Fig. 9(b) and (d) is the cross-sectional profile of the machined surface at 3 mm/min and 0.1 mm/min, respectively. A convex core appeared at the center with a certain height of residual material for both rough and fine grinding, which was attributed to the position error in the previous studies on machining spherical and aspherical surfaces [26, 27].

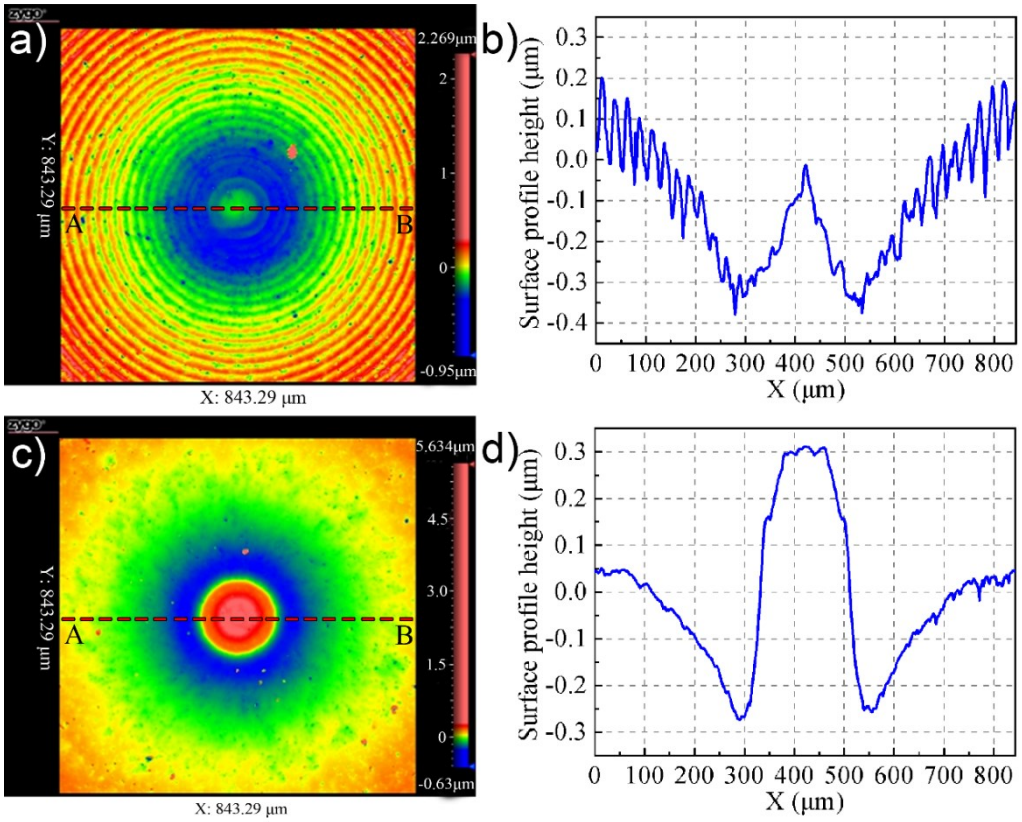

Fig. 9 3D topography and cross-sectional profile height of the machined surface at different feed rate: (a) and (b) for the feed rate of 3 mm/min; (c) and (d) for the feed rate of 0.1 mm/min

In the present work, a 60° sharp edge was firstly obtained by the diamond nib, and the sharp edge was then dressed by the Al_2O_3 stick to get an arc edge. Fig. 10 shows the edge profile of the diamond wheel after grinding. It can be readily seen that the sharp edge loss of the diamond wheel appears as the macro wheel wear. During the grinding process, the mechanical loads caused the removal of the surface material of the diamond wheel, resulting in the flattening of the arc edge. More specifically, profile deviation occurred along the feed direction. During the installation and adjustment of workpiece and grinding wheel, the wheel apex was firstly set in contact with the workpiece surface. Previous studies had reported that the center profile of machined surface would be affected by several error sources inevitably, such as the tool and workpiece setting error and position error [28-30]. Apart from the errors, it is found that the profile deviation of the grinding edge also contributes to the residual material at center, which results in the formation of a center cone, as shown in Fig. 9. The interaction model between the worn wheel and workpiece surface is illustrated in Fig. 11. Besides, due to the random fracture induced profile deviation of the wheel edge at varied processing parameters, the cone shape also varied at different grinding process.

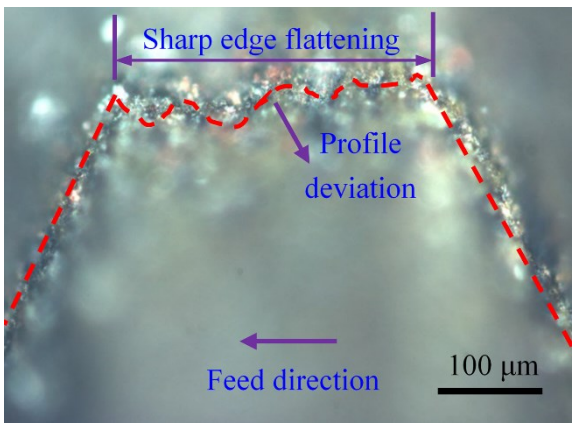

Fig. 10 The macro wheel wear after grinding

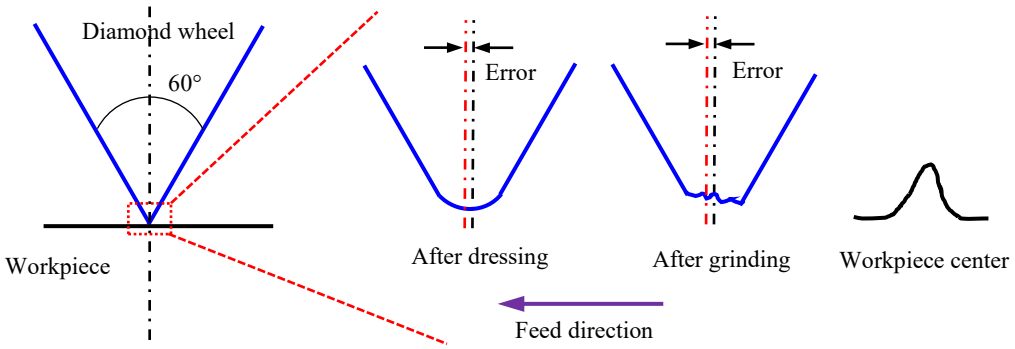

Fig. 11 Illustration of the impact of macro wheel wear and error on the form at center

In addition, a concave profile occurred just next to the conical core and the tool feed grooves were evident at 3 mm/min, but no obvious grooves formed at 0.1 mm/min. To illustrate the formation of the center profile, it is quite necessary to know the distribution of grinding points, that is, the interaction points between the diamond grits and the workpiece surface. In the present work, the workpiece rotated anticlockwise at a constant speed, with the diamond wheel moving from one side to the center, as shown in Fig. 1(b). The diamond grit with maximum cutting depth played a determined role on the surface profile [31], especially for the quick point grinding where the macro wheel wear resulted in the decreasing wheel roundness [32]. Therefore, the high spindle speed grinding process could be compared to raster milling in which the diamond grits participate in the material removal non-continuously. The distribution of the cutting points could be determined as by Eq. (4) to Eq. (7):

$$\begin{cases} x_i = r \cdot \cos(\omega \cdot t_i) \\ y_i = r \cdot \sin(\omega \cdot t_i) \end{cases} \tag{4}$$

$$t_i = \frac{i}{n_s} \tag{5}$$

$$r = R - f \cdot t_i \tag{6}$$

$$\omega = \frac{n_w}{60} \cdot 2\pi \tag{7}$$

where (x_i, y_i) is the coordinate position in X-Y system, n_s is the rotational speed of grinding wheel (RPM), n_w is the rotational speed of workpiece (RPM), f is the feed rate, R is the radius of workpiece, r is the radial position of grinding point, t is the time per rotation of wheel (t=1/n_s), T is the total time for one grinding pass (T=R/f), N is the total grinding points (N=T/t), i is the ith grinding point and ω is the angular speed of the workpiece. The simulated results at the two different feed rate are shown in Fig. 12. Helical tool path can be clearly found at the feed rate of 3 mm/min, while the high density of grinding points results in the non-clear separated feed marks at 0.1 mm/min (600×600 μm). Considering the shape and the high rotational speed of the diamond grinding wheel, the smaller radial distance from the center means the higher density and overlapping ratio of the cutting points. Therefore, the material removal volume increases with decreasing radial distance, resulting in the concave shape.

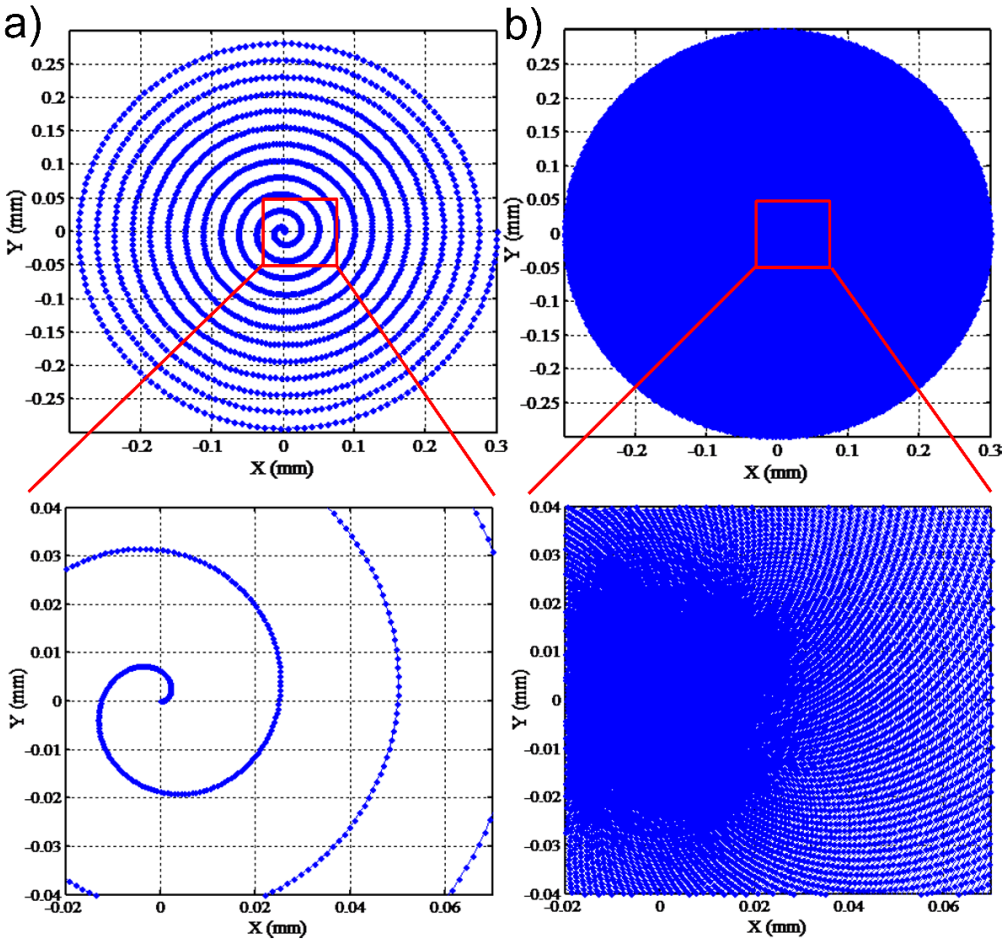

Fig. 12 Helical tool path and distribution of grinding points on the machined surface: (a) for 3 mm/min; (b) for 0.1 mm/min

4 Conclusions

In this study, the wheel wear mechanism and its impact on the nanometric surface characteristics of RB-SiC/Si under parallel diamond grinding are investigated. Based on the above analysis and discussion, the following conclusions could be achieved:

(1) With decreasing feed rate, the surface characteristics of RB-SiC/Si changed from surface fracture to be randomly distributed micro-pits at phase boundaries, and the surface finish also improved but with a limitation as the feed rate reached certain value;

(2) Micro wheel wear involved random grits splintering, abrasive wear, grain dislodgement and graphitization. Power spectrum analysis by Fast Fourier Transformation (FFT) of the surface profile data shows the determinant role of feed rate and micro wheel wear on the nanometric surface characteristics at finer feed rate, where random grits splintering contributed to the cluster spatial frequency at around 25 1/mm;

(3) Macro wheel wear occurred in the form of sharp edge flattening and profile deviation, which contributed to the formation of conical shape at the workpiece center. Simultaneously, the concave shape around the core was attributed to the higher density and overlapping ratio of cutting points which resulted in the high volume of material removal.

Acknowledgments

The work was partially supported by the National Natural Science Foundation of China (NSFC) (Project No.:51475109 and 51475119) and also the Research Committee of the Hong Kong Polytechnic University (RTRA).

Author contribution

Quanli Zhang performed the experiments and drafted the text. Qingliang Zhao and Suet To provide the financial supports, give instructions of the experiments and help do proof-reading of the draft. Bing Guo and Wenjie Zhai provide the technical instructions and help do proof-reading.

References

[1] E. Brinksmeier, Y. Mutlugünes, F. Klocke, J.C. Aurich, P. Shore, H. Ohmori, Ultra-precision grinding, CIRP Ann. - Manuf. Technol. 59 (2010) 652-671.

[2] H. Ohmori, W. Lin, J. Guo, Y. Uehara, S. Morita, N. Mitsuishi, K. Yoshikawa, M. Ohmori, K. Ikeda, T. Oku, T. Adachi, H.M. Shimizu, Fabrication process and

system for neutron refractive optics, Nucl. Instrum. Methods Phys. Res. Sect. A: Accel. Spectrom. Detect. Assoc. Equip. 529 (2004) 106-111.

[3] B. Denkena, L. Leon, B. Wang, Grinding of microstructured functional surfaces: a novel strategy for dressing of microprofiles, Prod. Eng. 3 (2009) 41-48.

[4] E. Savio, L. De Chiffre, R. Schmitt, Metrology of freeform shaped parts, CIRP Ann. - Manuf. Technol. 56 (2007) 810-835.

[5] H. Liang, X. Yao, H. Zhang, X. Liu, Z. Huang, Friction and wear behavior of pressureless liquid phase sintered SiC ceramic, Mater. Des. 65 (2015) 370-376.

[6] S. Chen, S. Lin, Study of an on-line precision microgroove generating process on silicon wafer using a developed ultra-thin diamond wheel-tool, Diam. Relat. Mater. 20 (2011) 339-342.

[7] K. Wegener, H.W. Hoffmeister, B. Karpuschewski, F. Kuster, W.C. Hahmann, M. Rabiey, Conditioning and monitoring of grinding wheels, CIRP Ann. - Manuf. Technol. 60 (2011) 757-777.

[8] M. Fujimoto, Y. Ichida, Micro fracture behavior of cutting edges in grinding using single crystal cBN grains, Diam. Relat. Mater. 17 (2008) 1759-1763.

[9] Y. Li, P.D. Funkenbusch, S.M. Gracewski, J. Ruckman, Tool wear and profile development in contour grinding of optical components, Int. J. Mach. Tool. Manuf. 44 (2004) 427-438.

[10] J.Y. Shen, J.Q. Wang, B. Jiang, X.P. Xu, Study on wear of diamond wheel in ultrasonic vibration-assisted grinding ceramic, Wear 332-333 (2015) 788-793.

[11] X. Sun, D.J. Stephenson, O. Ohnishi, A. Baldwin, An investigation into parallel and cross grinding of BK7 glass, Precis. Eng. 30 (2006) 145-153.

[12] Y. Liu, A. Warkentin, R. Bauer, Y. Gong, Investigation of different grain shapes and dressing to predict surface roughness in grinding using kinematic simulations,

Precis. Eng. 37 (2013) 758-764.

[13] G. Spur, S.E. Holl, Ultrasonic assisted grinding of ceramics, J. Mater. Process. Technol. 62 (1996) 287-293.

[14] B. Chen, B. Guo, Q. Zhao, An investigation into parallel and cross grinding of aspheric surface on monocrystal silicon, Int. J. Adv. Manuf. Technol. (2015) 1-10.

[15] R. Narulkar, S. Bukkapatnam, L.M. Raff, R. Komanduri, Graphitization as a precursor to wear of diamond in machining pure iron: a molecular dynamics investigation, Comp. Mater. Sci. 45 (2009) 358-366.

[16] Y.G. Gogotsi, A. Kailer, K.G. Nickel, Materials: transformation of diamond to graphite, Nature 401 (1999) 663-664.

[17] Q. Zhang, S. To, Q. Zhao, B. Guo, Amorphization and C segregation based surface generation of Reaction-Bonded SiC/Si composites under micro-grinding, Int. J. Mach. Tool. Manuf. 95 (2015) 78-81.

[18] L. Yin, H. Huang, Brittle materials in nano-abrasive fabrication of optical mirror-surfaces, Precis. Eng. 32 (2008) 336-341..

[19] Q. Zhang, S. To, Q. Zhao, B. Guo, G. Zhang, Impact of material microstructure and diamond grit wear on surface finish in micro-grinding of RB-SiC/Si and WC/Co carbides, Int. J. Refract. Met. Hard Mater. 51 (2015) 258-263.

[20] Z. Xie, R.J. Moon, M. Hoffman, P. Munroe, Y. Cheng, Role of microstructure in the grinding and polishing of α-sialon ceramics, J. Eur. Ceram. Soc. 23 (2003) 2351-2360.

[21] Z.H. Xie, M. Hoffman, R.J. Moon, P.R. Munroe, Y.B. Cheng, Sliding wear behaviour of Ca α-sialon ceramics at 600°C in air, Wear 260 (2006) 1356-1360.

[22] D. Axinte, P. Butler-Smith, C. Akgun, K. Kolluru, On the influence of single grit micro-geometry on grinding behavior of ductile and brittle materials, Int. J. Mach.

Tool. Manuf. 74 (2013) 12-18.

[23] G. Chen, S. Cai, C. Zhou, On the laser-driven integrated dressing and truing of bronze-bonded grinding wheels, Diam. Relat. Mater. 60 (2015) 99-110.

[24] Z.B. Hou, R. Komanduri, On the mechanics of the grinding process - Part I. Stochastic nature of the grinding process, Int. J. Mach. Tool. Manuf. 43 (2003) 1579-1593.

[25] B. Guo, Q. Zhao, H. Li, Ultraprecision grinding of TiC-based cermet hemisphere couples, Int. J. Adv. Manuf. Technol. 73 (2014) 1281-1289.

[26] F. Chen, S. Yin, H. Ohmori, J. Yu, Form error compensation in single-point inclined axis nanogrinding for small aspheric insert, Int. J. Adv. Manuf. Technol. 65 (2013) 433-441.

[27] Y. Hwang, T. Kuriyagawa, S. Lee, Wheel curve generation error of aspheric microgrinding in parallel grinding method, Int. J. Mach. Tool. Manuf. 46 (2006) 1929-1933.

[28] Brinksmeier, E.; Oltmann, R.; Kai, R.; Kathrin. Kinematics in ultra-precision grinding of WC moulds. Int. J. of Nanomanufacturing 7 (2011) 199-213.

[29] H. Huang, W.K. Chen, T. Kuriyagawa, Profile error compensation approaches for parallel nanogrinding of aspherical mould inserts, Int. J. Mach. Tool. Manuf. 47 (2007) 2237-2245.

[30] M. Chen, Q. Zhao, S. Dong, D. Li, The critical conditions of brittle–ductile transition and the factors influencing the surface quality of brittle materials in ultra-precision grinding, J. Mater. Process. Technol. 168 (2005) 75-82.

[31] B. Guo, Q. Zhao, On-machine dry electric discharge truing of diamond wheels for micro-structured surfaces grinding, Int. J. Mach. Tool. Manuf. 88 (2015) 62-70.